Tellus (2008), 60A, 528–546
Printed in Singapore. All rights reserved

TELLUS

Optimal atmospheric forcing perturbations for the cold-ocean warm-land pattern

By T. IVERSEN[1,2]*, J. KRISTIANSEN[1], T. JUNG[3] and J. BARKMEIJER[4], [1]*Norwegian Meteorological Institute, Oslo, Norway;* [2]*Department of Geosciences, University of Oslo, Norway;* [3]*European Centre for Medium-Range Weather Forecasts, Reading, United Kingdom;* [4]*Royal Netherlands Meteorological Institute, De Bilt, the Netherlands*

(Manuscript received 1 May 2007; in final form 19 December 2007)

ABSTRACT

The atmospheric Integrated Forecast System model from the European Centre for Medium-Range Weather Forecasts is used to calculate forcing perturbations which are optimal in producing atmospheric response patterns resembling the 'cold-ocean-warm-land' (COWL) flow regime over 4 d. Similar initial state perturbations are computed for comparison. COWL is relevant for recent climate change. The perturbations are optimal in a tangent-linear sense but are validated by non-linear calculations. Calculations cover 836 cases during 22 winter seasons. The method effectively estimates flow-dependant perturbations which produce response patterns resembling COWL. The optimal forcing is more geographically confined with relatively smaller remote amplitudes and larger spatial scale than the initial state perturbations. The quality of the 4-d response is highly dependent on the actual optimal perturbation. Averaging over just a few cases drastically reduces this optimal property, but the long-term climate response of an average forcing does produce signatures of the COWL regime. The results are discussed in view of Palmer's non-linear dynamical perspective on climate change, and several key elements are confirmed: the climate sensitivity is flow dependent; efficient forcing structures do not resemble the response (non-normality); sensitivity and predictability are negatively correlated; and flow characteristics for high sensitivity differ from those for low sensitivity.

1. Introduction

In this paper we estimate and discuss optimal external forcing structures that favour subsequent large-scale atmospheric circulations which project onto the cold-ocean-warm-land (COWL) flow regime. A geographical pattern associated with COWL was identified by Wallace et al. (1996) as regression coefficients between atmospheric anomalies in either of the geopotential heights of 1000 or 500 hPa, and anomalies in monthly temperatures averaged over the Northern Hemisphere (NH) land surface for the cold-season (November–April). This pattern was used to separate a 20th century multidecadal warming trend from a presumed dynamically contributed intraseasonal and interannual variability in the NH surface temperature. Despite being defined through surface temperature anomalies, the COWL pattern had a deep equivalent-barotropic structure with decreasing temperature amplitudes with height. Broccoli et al. (1998) found evidence of the COWL pattern as a natural mode of climate variability in a 1000 yr long control simulation of the coupled global climate model at the Geophysical Fluid Dynamics Laboratory (GFDL).

It is a matter of some debate to what extent flow regimes and multimodal probability density functions (pdf) of atmospheric states are well defined (e.g. Stephenson et al., 2004). It is nevertheless possible to identify persistent flow anomalies (Branstator, 1990) or synoptically defined patterns that are recognized by its high degree of persistence, despite showing slightly different characteristics between each occurrence (e.g. Jung et al., 2005). Extratropical blocking is a well documented regional phenomenon associated with persistent flow anomalies (Rex, 1950; Blackmon, 1976; Lejenäs and Økland, 1983; Kanestrøm et al., 1985). Some flow patterns are associated with teleconnections (Wallace and Gutzler, 1981) such as the Pacific-North American pattern (PNA) and the North-Atlantic oscillation (NAO; Hurrel, 1996).

The hemispheric scale of these patterns and their possible nature as dynamical modes of variability, that is, flow regimes, are less well established. No significant covariance between Atlantic and Pacific blocking has been revealed (Lejenäs and Økland, 1983) and the PNA and NAO patterns appear to fluctuate independently for much of the time (Wallace et al., 1996). On the other hand, early cluster analyses pointed out statistically

*Corresponding author.
e-mail: trond.iversen@met.no
DOI: 10.1111/j.1600-0870.2008.00310.x

significant hemispheric-scale flow patterns (Mo and Ghil, 1988; Molteni et al., 1990). Furthermore, both Kimoto and Ghil (1993) and Cheng and Wallace (1993) found a hemispheric COWL pattern from cluster analysis in a truncated phase space spanned by the two leading empirical orthogonal functions (EOF) of free tropospheric flow maps. These results are complemented by several recent studies (Corti et al., 1999; Smyth et al., 1999; Lu et al., 2004, Quadrelli and Wallace, 2004; Wu and Straus, 2004a, b) which all identify common hemispheric patterns of COWL interpreted as atmospheric modes of variability. Similar results are found for the Northern Annular Mode (NAM), that is, the Arctic Oscillation (AO; Thompson and Wallace, 1998, 2000), and the PNA. In this work, we use these hemispheric patterns as signatures of flow regimes, realizing that more significant results probably could be achieved by using sector patterns. See Molteni et al. (2006) for a further discussion of the significance of clusters and their similarities.

One important motivation for this study is to investigate major aspects of the non-linear dynamical perspective put forward by Palmer (1993, 1999) and discussed in Palmer (1996). This perspective challenges the view that anthropogenic climate change should deviate considerably from natural variability and thus be recognized as 'fingerprints' of the forcing causing it (e.g. Hasselmann, 1993). It provides concepts for the atmospheric response to a small imposed forcing, given that the atmosphere behaves as a non-linear and unstable dynamical system. Instability is manifested by the fact that arbitrary close states diverge and yield a strange attractor. Palmer (1999) identifies two basic aspects of non-linearity. First, non-linearity causes the rate at which close states diverge to vary with the actual position on the attractor, or alternatively that the atmospheric predictability depends on the actual weather. Existence of dynamical flow regimes characterized by quasi-stationary synoptic patterns with increased predictability can thus be understood in view of this property of non-linearity. However, extended predictability can also be associated with developments under swift transition (see discussion in section 4 of Corti and Palmer 1997). The second aspect of non-linearity concerns the non-normal property of the tangent-linear model caused by the linearization of non-linear terms such as advection. The non-normality leads to non-orthogonal normal modes and, as thoroughly discussed in Farrel and Ioannou (1996a, b), arbitrary perturbations may grow over finite time intervals even though the amplitudes of all normal modes decrease and the system as such is characterized as stable.

Flow regimes and flow-dependent predictability are basic concepts in the non-linear dynamical perspective, which can be summarized in a few points: (i) the impact of a small imposed forcing is felt primarily when predictability is small; (ii) the climate response to a small imposed forcing is primarily manifested in terms of changes in the frequency of occurrence of flow regimes; (iii) the geographical structure of the flow regimes is relatively unaffected by the small imposed forcing and (iv) the influence

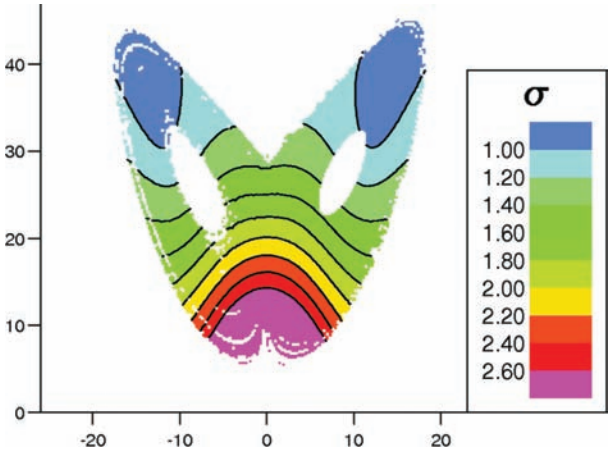

Fig. 1. Leading singular values calculated over an optimization time typically required for a shift between the regimes in the Lorenz (1963) chaotic model (60 dimensionless time units). The values are plotted for starting points on the attractor and are depicted in the *xz*-plane, where *x* and *z* are the standard dimensionless co-ordinates of the model. The imposed constant forcing of 4.5 dimensionless units points from the left fix-point (C−) to the right (C+) in the middle of the two 'holes'. Values larger than 1.0 signify that adjacent states will diverge over the next 60 time units, and the system is highly sensitive for the imposed forcing when the singular values are large (red colours). The short-term predictability is small in the red area (e.g. Nese, 1989), where the system is sensitive to the forcing. The system's response to the forcing is a higher number of states around the fix point C+ (on the right-hand side) than around C− (on the left-hand side).

of the small imposed forcing may be strongest in localized regions which will not coincide with the regions of atmospheric response. One consequence of this perspective is that a region's climate change should be determined by the properties of the naturally occurring flow regimes that change their frequency of occurrence, rather than by the details of the forcing. Boer and Yu (2003) came to similar conclusions, by discussing the climate response to an imposed forcing in terms of internal feedbacks rather than non-linear dynamics. Their view appears to depend less on the existence of flow regimes, but atmospheric non-linear dynamics (advection) is nevertheless an important vehicle for provoking remote feedback.

The three-variable equations of Lorenz (1963) can serve as an illustration. A constant external forcing is added to the equations with positive components for the *x*- and *y*-variables. Figure 1 shows that the hole in the middle is much larger on the left wing than the right, and there are also more open spaces on the left wing. As expected, the response is that more states belong to the right 'regime' of the attractor than the left, although a considerable fraction of the states respond negligibly to the external forcing (see also fig. 2a in Palmer 1999). Over a time-interval of typical transitions between the regimes (60 time-units), the system is very sensitive to such a forcing for states in the lower portion of the attractor, where the predictability is known to be at its minimum. Considerably more than 50% of states that visit

this sensitive part of the attractor subsequently select the right regime. Apart from the different number of states in the two regimes which occur in response, the shape of the attractor is practically insensitive to the forcing. The pattern of states that define the response is indeed very different from those states which feel the impact of the forcing.

Corti et al. (1999) detected a positive trend in the relative occurrence of COWL, and a simultaneous negative trend in the relative occurrence of AO in its negative phase, in the latter half of the 20th century. Hence aspects of the observed climate change in the NH can be interpreted as a systematic change in the pdf of atmospheric states associated with COWL and AO, without any significant change in their geographical structure. In this respect Corti et al. (1999) showed that Palmer's non-linear dynamical perspective may offer a valuable interpretation of the observed climate change over the latter half of the 20th century in response to a possibly anthropogenic external forcing. The results of forced experiments with the GFDL climate model discussed in Broccoli et al. (1998) can also be interpreted in view of the non-linear perspective.

Inspired by the analysis of Corti et al. (1999) and the non-linear dynamical perspective of Palmer (1993, 1999), we use a state-of-the-art global numerical weather prediction model to construct forcing sensitivity patterns (FSP) for COWL. We define the FSP for COWL at time t as the constant forcing of a given magnitude which produces an atmospheric response with maximum COWL index (CI) when imposed on the atmosphere over a specified time interval $[t,\ t + T]$. Note that the forcing is constant over each time interval, but varies from case to case. The CI of the response is the projection of the resulting increment on the atmospheric state on the COWL pattern. The shape of the FSP for COWL and any well defined COWL sensitivity index (CSI), will vary from case to case due to non-linearity.

The FSP may represent tendencies in mass, momentum, or energy due to exchange through the upper and lower boundaries, or from internal atmospheric processes. Its significance will be discussed in light of Palmer's non-linear dynamical perspective. Thus, a real forcing which projects positively onto the FSP for COWL when sensitivity is high, should increase the occurrence of COWL compared to flow regimes which are not correlated with COWL. It is well documented that the NH pattern of increased observed surface air temperature during the last 50 years is closely related to COWL (Randall et al., 2007). In this regard we set forth to study the relevance of COWL as a dynamical mode of NH atmospheric variability, and as a signature of climate change. The relation between a known external forcing and the calculated FSP is not addressed, but is subject for further study (see also Moore et al., 2006). Similarly, we do not discuss physical mechanisms for onset or decay of quasi-persistent flow patterns as, for example, done by Evans and Black (2003).

In this study we use a relatively recent version (cycle 29r2) of the Integrated Forecast System (IFS) from the European Centre for Medium-Range Weather Forecasts (ECMWF). The skill of medium-range forecasts by the IFS has been substantially improved during the last decades (Simmons and Hollingsworth, 2002), including a reduction in systematic errors (Jung, 2005; Uppala et al., 2005). Although models of this kind are not perfect replicas of the atmosphere, we can regard them as the most reliable laboratories in the search for atmospheric FSPs.

This paper follows up preliminary studies by Iversen et al. (2003, 2006). The method for calculating FSP is an extension of eq. (16) in Palmer (1999). The method was originally designed to diagnose key model tendency errors that reduce short to medium range predictability on a given day (Barkmeijer et al., 2003). Related results were presented for initial state sensitivity patterns (ISP) for sector flow regimes by Oortwijn and Barkmeijer (1995) and Corti and Palmer (1997), and for FSP of hemispheric patterns by Iversen et al. (2003), using a much simpler three-level quasi-geostrophic model. Jung and Barkmeijer (2006) carried out similar experiments as presented here with the ECMWF IFS, but for stratospheric forcing of AO and a much smaller sample size.

The paper starts with a short description of methods, definitions, and data in Section 2. In Section 3, we present the FSP, ISP and CSI calculations. Response patterns to the FSP and ISP are presented and discussed in Section 4. In Section 5, we discuss the non-linear dynamical perspective of Palmer (1993, 1999). A summary and some conclusions are given in Section 6.

2. Methodology and definitions

2.1. *The model and basic data*

The experimental tool in this study is the cycle 29r2 of the ECMWF IFS global numerical weather prediction model, which was used operationally from 28 June 2005 to 1 February 2006 (see www.ecmwf.int/research/ifs/). There are 60 levels in the vertical of which about half are located above the tropopause and below ca. 0.1 hPa. In this study the so-called sensitivity suite (Klinker et al., 1998) of the model is used. Due to computational costs a reduced spectral resolution of T63 is employed for non-linear control and perturbation runs. This corresponds to about 1.875° on a regular latitude–longitude grid or a N48 Gaussian grid, which is amongst the finer resolution of the atmosphere in present climate models. For consistency, the tangent linear model and its adjoint use the same resolution.

The basic fields of meteorological data and sea surface temperatures are taken from the ERA-40 re-analysis (Uppala et al., 2005) which covers the period from September 1957 to August 2002. We select data from 22 extended winter seasons between mid-October and mid-April. Within these periods, the 4-d sensitivities and FSPs are normally calculated every fifth consecutive day, yielding 38 selected dates for each season and a total of 836 individual cases. For shorter periods calculations were made more frequently to investigate the duration of sensitivity anomalies.

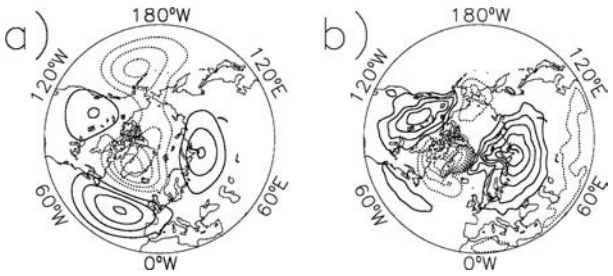

Fig. 2. The COWL flow pattern generated from Corti et al. (1999). (a) 500 hPa geopotential height anomaly with equidistance 20 m. (b) Temperature with equidistance 0.6 K, at model level 60 close to the ground surface.

2.2. *The COWL regime and COWL index*

It is assumed that the anomaly pattern defined as COWL represents a dynamical mode of variability in the atmosphere during the NH winter. We refer to this mode as the 'COWL regime'. Our estimated anomalies in the 500 hPa geopotential height for the COWL regime are presented in Fig. 2a. They are based on the cluster A in Corti et al. (1999). We have extended this anomaly pattern to the full set of atmospheric state variables in the ECMWF IFS model except humidity, by performing a weighted average of the ERA-40 monthly data (Uppala et al., 2005). The weights are normalized projection coefficients of monthly 500 hPa anomalies of unit length onto the original cluster A pattern. These projections are calculated with the standard Euclidian inner product. The thus obtained air temperature at the lowest model level is shown in Fig. 2b. The temperature anomalies are smaller at 500 hPa (not shown).

There are many examples of atmospheric flow indices in the literature based on synoptic characteristics (e.g. Rex, 1950), teleconnections (e.g. Wallace and Gutzler, 1981) and cluster analysis in a phase space of reduced dimensions (e.g. Molteni et al., 1990). In this paper, we define the CI of a given atmospheric state at time t, x_t, in terms of the projection of the associated anomaly field onto the COWL regime pattern:

$$\mathrm{CI}\,(x_t) = \frac{\langle x_t - \mathbf{c},\, \mathbf{C_T}\gamma_{\mathrm{COWL}}\rangle}{\langle \gamma_{\mathrm{COWL}},\, \mathbf{C_T}\gamma_{\mathrm{COWL}}\rangle}, \tag{1}$$

where $\mathbf{c}$ is the state vector for the monthly average atmospheric climate defined over the entire ERA-40 data, and γ_{COWL} is the anomaly pattern for the COWL regime. The expression $\langle \mathbf{x}, \mathbf{y}\rangle$ denotes the standard Euclidian inner product, and $\mathbf{C}_{\mathrm{T}}$ is a positive definite and symmetric matrix that defines the type of norm. We choose an inner product which produces a norm in terms of total energy (Buizza and Palmer, 1995; Ehrendorfer et al., 1999), but the properties of CI do not depend critically on the choice of norm. Both the 500 hPa metric norm (Oortwijn and Barkmeijer, 1995) and the kinetic energy norm (Corti and Palmer, 1997; Iversen et al. 2003) give similar results for a three-level quasi-geostrophic model. Note that the CI in eq. (1) measures both the resemblance in spatial pattern and the anomaly amplitude.

The hemispheric COWL regime includes a pattern of a positive phase NAO. NAO is normally regarded as a sector anomaly pattern which relates to the hemispheric-scale AO (Wallace, 2000). Cluster D in Corti et al. (1999) is dominated by a pattern with negative-phase AO and hence a negative NAO index. A time-series of CI will be negatively correlated with a simultaneous time-series of an index for cluster D. On the other hand, a similar index for their cluster B, which is dominated by a negative phase PNA, is not expected to produce significant correlation with CI.

2.3. *Estimating the COWL sensitivity pattern and sensitivity index*

We seek perturbations $\bar{\mathbf{f}}$ of the atmospheric forcing (or ε_0 of the initial state) that produce a state difference ε_T compared to the control state $\mathbf{x}^c_{\mathrm{T}}$ at final time T, which is as close as possible to the anomaly pattern $\gamma = \mathrm{A}\,\gamma_{\mathrm{COWL}}$. Here A is a constant number discussed in Section 2.4 below. Thus, perturbations $\bar{\mathbf{f}}$ (or ε_0) should minimize the cost function:

$$J = \frac{1}{2}\,\langle \mathbf{P}(\varepsilon_{\mathrm{T}} - \gamma),\ \mathbf{C_T}\mathbf{P}(\varepsilon_T - \gamma)\rangle\,, \tag{2}$$

where $\varepsilon_{\mathrm{T}} = \mathbf{x_T} - \mathbf{x^c_T}$. Here, $\mathbf{P}$ is a local projection operator (Buizza, 1994) which excludes points outside the extra-tropical NH. We approximate ε_{T} in (1) by the resulting tangent linear evolution over the optimization time interval $[t,t+T]$ relative to the non-linear control development $\mathbf{x}^c_t$ calculated with the full ECMWF IFS model. Expressed by the resolvent:

$$\varepsilon_T = \mathbf{M}\,(0,\mathrm{T})\,\varepsilon_0 \tag{3a}$$

for initial state perturbation, and:

$$\varepsilon_T = \tilde{\mathbf{M}}\,(0,\mathrm{T})\,\bar{\mathbf{f}} \tag{3b}$$

for constant forcing perturbations. Here $\mathbf{M}$ (0, T) is the tangent-linear propagator, and $\tilde{\mathbf{M}}(0,\mathrm{T}) = \int_0^T \mathbf{M}(\mathrm{s},\mathrm{T})\mathrm{ds}$. Both operators depend on the actual state, which is the first aspect of non-linearity discussed in Palmer (1999). See Barkmeijer et al. (2003) and Jung and Barkmeijer (2006) for further details about their calculation.

We define the initial sensitivity pattern (ISP) as the pattern $\boldsymbol{\varepsilon_0}$ which minimizes J given (3a), and the FSP as the pattern $\bar{\mathbf{f}}$ which minimizes J given (3b). These patterns are approximately estimated by an iterative procedure (Barkmeijer et al., 2003) which requires estimates of the phase space gradient of J with respect to $\boldsymbol{\varepsilon_0}$:

$$\nabla_0 \mathrm{J} = \mathbf{C}_0^{-1}\mathbf{M}^*\mathbf{P}^*\mathbf{C}_{\mathrm{T}}\mathbf{P}(\mathbf{M}\varepsilon_0 - \gamma) \tag{4a}$$

or with respect to $\bar{\mathbf{f}}$:

$$\nabla_{\mathrm{f}} \mathrm{J} = \mathbf{C}_0^{-1}\tilde{\mathbf{M}}^*\mathbf{P}^*\mathbf{C}_{\mathrm{T}}\mathbf{P}(\tilde{\mathbf{M}}\bar{\mathbf{f}} - \gamma). \tag{4b}$$

The adjoints $\mathbf{M}^*$, $\tilde{\mathbf{M}}^*$ and $\mathbf{P}^*$ are defined with respect to the Euclidian inner product. Due to linearized advection terms, which

are non-linear originally, in general cases $\mathbf{M}$ and $\tilde{\mathbf{M}}$ are not normal ($\mathbf{M}^*\,\mathbf{M} \neq \mathbf{M}\mathbf{M}^*$) and their eigenvectors, the normal modes, are not orthogonal. This is the second aspect of non-linearity discussed by Palmer (1999). The symmetric and positive definite operator $\mathbf{C}_0$ allows a different norm initially than at final time T. The procedure for finding FSP estimates for each iteration an increment $\delta\bar{\mathbf{f}}$ along the former estimate of the gradient (4b) which is constrained by keeping $\langle \mathbf{C_0}\delta\mathbf{f}, \delta\mathbf{f} \rangle$ constant. Initial state increments $\boldsymbol{\delta\varepsilon_0}$ are estimated analogously keeping $\langle \mathbf{C_0}\,\boldsymbol{\delta\varepsilon_0}, \boldsymbol{\delta\varepsilon_0}\rangle$ constant. The iterative procedure starts by assuming $\bar{\mathbf{f}} = 0$ in (4b), (or $\varepsilon_0 = 0$ in eq. 4a) yielding $[\nabla_0 \mathbf{J}]^0 = -\mathbf{C}_0^{-1}\mathbf{M}^*\mathbf{P}^*\mathbf{C}_T\mathbf{P}\gamma$ and $[\nabla_{\mathrm{f}} \mathrm{J}]^0 = -\mathbf{C}_0^{-1}\tilde{\mathbf{M}}^*\mathbf{P}^*\mathbf{C}_T\mathbf{P}\,\gamma$. We define the CSI with respect to forcing by:

$$CSI = \frac{1}{\mathrm{T}} \left\| [\nabla_{\mathrm{f}} \mathrm{J}]^0 \right\|_{\mathrm{C}_0} \cdot \|\gamma\|_{\mathrm{C}_0}^{-1} \tag{5}$$

and similar with respect to initial state: $CSI^* = \|[\nabla_0 \mathbf{J}]^0\|_{\mathrm{C}_0} \cdot \|\gamma\|_{\mathrm{C}_0}^{-1}$. The norm of a state vector $\mathbf{y}$ is defined as $\|\mathbf{y}\|_{\mathrm{C}_0} = \langle \mathbf{y}, \mathbf{C_0}\mathbf{y}\rangle^{1/2}$ and T is the optimization time.

Through $\mathbf{M}$ and $\tilde{\mathbf{M}}$ the sensitivities depend on the actual system state. Klinker et al. (1998) designed the iteration procedure for initial state sensitivities for γ equal to a short-term forecast error, and Barkmeijer et al. (2003) did the same for forcing sensitivities. Here we apply the methods to anomaly patterns associated with atmospheric flow regimes such as COWL. Klinker et al. (1998) showed that three iterations yield a best fit to the observations for adiabatic computations (Buizza, 1993). According to Jung et al. (2003) six iterations appear to be necessary for diabatic adjoint calculations due to slower convergence, and that is our choice. The linear physics in the diabatic tangent-linear and adjoint models is described by Mahfouf (1999) and comprises vertical diffusion, subgrid scale orographic effects, large-scale condensation, long-wave radiation and deep cumulus convection. Note that the side condition of constant norm of the iteration increments will, together with the number of iterations, determine the norm of the full FSP and ISP as well as their tangent-linear evolution. The evolved patterns' norm will in general differ from the norm of the anomaly pattern γ.

2.4. *Some parameter choices*

Details of the adjoint model influence the results, and since the adjoints in (4) depend on the norm, so will the sensitivities. The total energy norm (e.g. Barkmeijer et al., 2003) gives a reasonably complete picture of the differences between atmospheric states (e.g. Orrell et al., 2001; Orrell, 2002). Our target domain defined by $\mathbf{P}$ in (2) is the part of the NH north of 30°N. Except for some special tests, the FSP or ISP are not restricted to any geographical region or vertical levels by $\mathbf{C}_0$, and all the model variables except specific humidity, are included in the optimization procedure.

The COWL anomaly pattern is multiplied by a scalar factor A, hereafter denoted the regime pattern scaling factor, that is, $\gamma = \mathrm{A}\gamma_{\mathrm{COWL}}$ in (2). The pattern γ_{COWL} is derived from monthly data, and its amplitude is inflated since the daily experiments features structures of much larger amplitudes. Note that although the CSI (6) does not depend on A, it may nevertheless influence the linearity. Except for a few cases we have chosen $A = 10$. Experiments with $A = 1$, 2.5, 10 or 40 reveal that the ability to produce a response resembling the COWL regime pattern increases with A, but for $A > 10$ the increase is modest (Iversen et al., 2006), probably because of non-linear effects.

The optimization time T should capture the typical duration of flow regime transitions for COWL. Transition times are typically much shorter than the average residence time of states belonging to the regimes. For instance, for strongly coupled flow regimes like ENSO the time-scale may be weeks to a few months (Moore and Kleeman, 1999). Predominantly, atmospheric regime switches, such as between mid-latitude zonal flows and blocking, may occur within a few days. In this paper, we assume $T = 4$ d as a suitable time range for the NH atmospheric regimes, even though this optimization time may limit potential remote influences such as possibly systematic transient wave-trapping downstream over vast distances (Branstator, 2002). Pacific SST perturbations such as associated with ENSO have a tendency to increase the frequency of COWL events on monthly, interannual (Molteni et al., 1993), and decadal (Kumar and Hoerling, 1998) timescales. Nevertheless, a considerably larger optimization time T would increase the pattern's dependence on details in the actual atmospheric flows (see discussion in Palmer, 1999).

2.5. *The estimated non-linear response*

The method's success is mainly defined by the degree of resemblance between the non-linear atmospheric response of the sensitivity patterns and the COWL anomaly pattern. Once a FSP ($\bar{\mathbf{f}}$) has been determined, its impact on the atmospheric state development is calculated by adding $\bar{\mathbf{f}}$ as a forcing term to the IFS model and produce a fully non-linearly evolved pattern over time interval $[t, t + T]$. The evolved ISP perturbations are similarly calculated by integrating the unperturbed IFS starting from $\boldsymbol{x}_0 + \boldsymbol{\varepsilon}_0$. The difference between the results from the perturbed runs and the unperturbed control forecast ($\boldsymbol{x}_{\mathrm{t}} - \boldsymbol{x}_{\mathrm{t}}^c$) at any future time t is the non-linear response to the FSP (or alternatively the ISP). The validity of the procedure of finding $\bar{\mathbf{f}}$ and ε_0 is tested by comparing the results of the non-linear response at time T ($\boldsymbol{x}_{\mathrm{T}} - \boldsymbol{x}_{\mathrm{T}}^{\mathrm{c}}$) with the COWL regime pattern (γ_{COWL}).

In cases when the non-linear response has little resemblance with the COWL regime, one reason could be that the tangent-linear assumption is poor for the chosen perturbation amplitude. This is also influenced by the chosen length of the optimization interval, T, (e.g. Errico, 1997), since reduced amplitudes of the FSP or ISP may become necessary in order to keep the response quasi-linear throughout the time span T. The iterative procedure

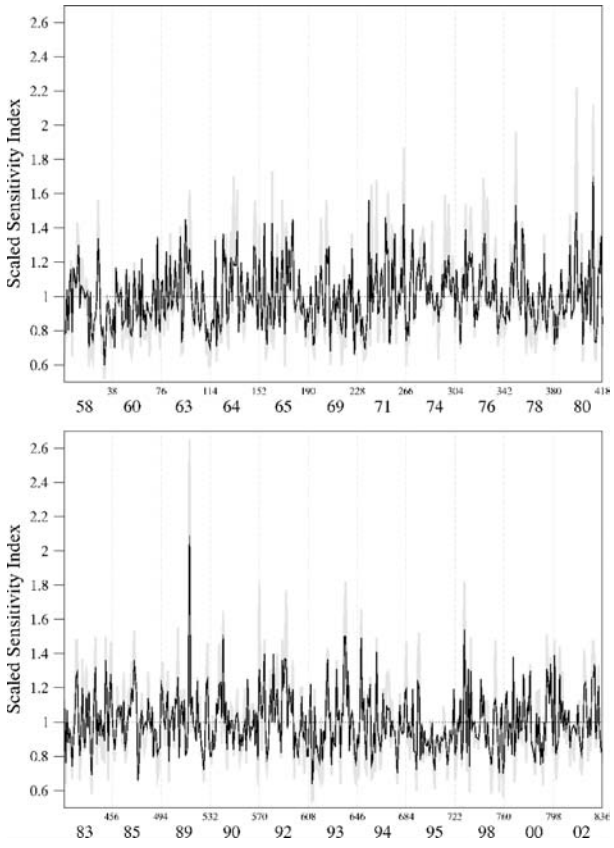

Fig. 3. Daily values of the COWL sensitivity index (CSI) for initial state (thin, sample average 11.48) and for forcing (thick, sample average 2.66) (see eq. 5) for 22 extended winter seasons. The sensitivity values are scaled by dividing with the respective sample averages, and values assigned to day D is for the optimization time interval [D, D + 4 d]. The sensitivities are calculated every 5 d, except for some selected periods highlighted in Fig. 5. The sample correlation coefficient between the two sensitivity indices is 0.91.

designed by Ortwijn and Barkmeijer (1995) could then be used, in which the non-linear control forecast $\mathbf{x}_t^c$ is redefined for each iteration by adding the small amplitude increments proportional to either FSP or ISP determined as described in Section 2.3. We have not found this to be necessary in our experiments.

3. Estimated atmospheric sensitivity

3.1. The COWL sensitivity index

The CSI (see eq. 5) is shown as a function of time in Fig. 3 and as frequency distribution histograms in Fig. 4. A few selected periods and cases are studied with higher temporal resolution, as shown in Fig. 5. The two series of CSI for initial state and forcing, respectively, are made comparable by normalization, that is, each individual CSI is divided with the sample average of each series. Only very few cases have considerably higher sensitivity than average, such as on 26 January 1989. The frequency distributions of normalized CSI are slightly skewed with a longer tail in the direction of high values (i.e. high sensitivities). The temporal correlation between the initial state and forcing CSIs amounts to as much as 0.91. Of the 20% most (least) sensitive cases to forcing, 78% (72%) occurred on the same day as the 20% most (least) sensitive cases to initial perturbations. The initial state CSI has larger variability than the forcing CSI, and the frequency distribution is slightly more skewed with more pronounced peak sensitivities.

Both the initial state and forcing CSIs have negligible temporal autocorrelation. This is also seen when CSI is calculated more frequently, and a closer inspection of the two highest peaks shown in Fig. 5 (26 January 1989 and 14 March 1980) reveals that on consecutive days before and after each of the peaks the sensitivities are considerably smaller. This indicates that the atmosphere can be sensitive to weak perturbations during time slots of only a day or two. This reflects (but does not prove) that atmospheric perturbations become increasingly dependent on details in the atmospheric flow as described by the propagators $\mathbf{M}$ and $\tilde{\mathbf{M}}$ (eq. 3) when the optimization time T increases (Palmer, 1999). On the other hand, as $T \to 0$ then $\bar{\mathbf{f}}$ and ε_0

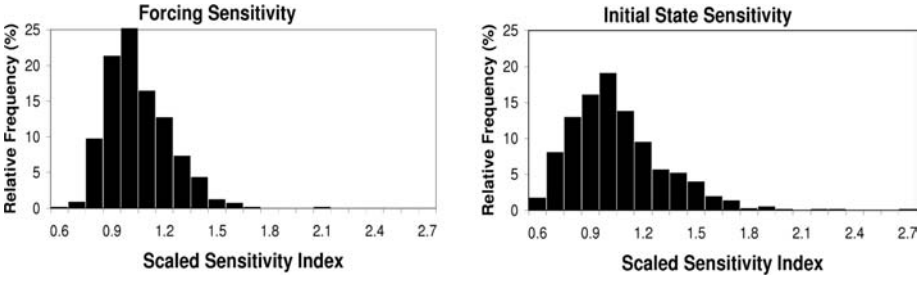

Fig. 4. Frequency distribution histograms for the sensitivity indices of Fig. 3 (for the 1985 winter only half the data points are used, i.e., every 5 d); forcing sensitivity (left) and initial state sensitivity (right). All class intervals are of equal length and the first interval includes sensitivity indices in the range 0.50005–0.60005. Both the horizontal and vertical axes are the same in both figures. The medians are 0.97 and 0.95 for the left and right figures, respectively. The 20% most sensitive forcing cases lay above 1.1540 and the 20% least below 0.8494. For the initial state sensitivities the corresponding values are 1.18790 and 0.7805, respectively.

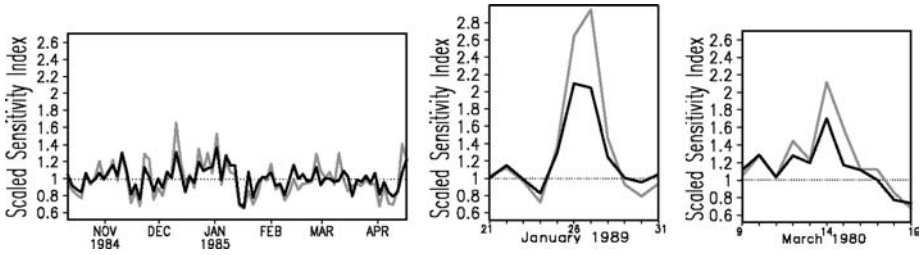

Fig. 5. Details from the panels in Fig. 3. The panel to the show selected periods for which sensitivities are calculated twice per 5 d. The two panels to the right highlight two very sensitive cases for which sensitivities are calculated daily.

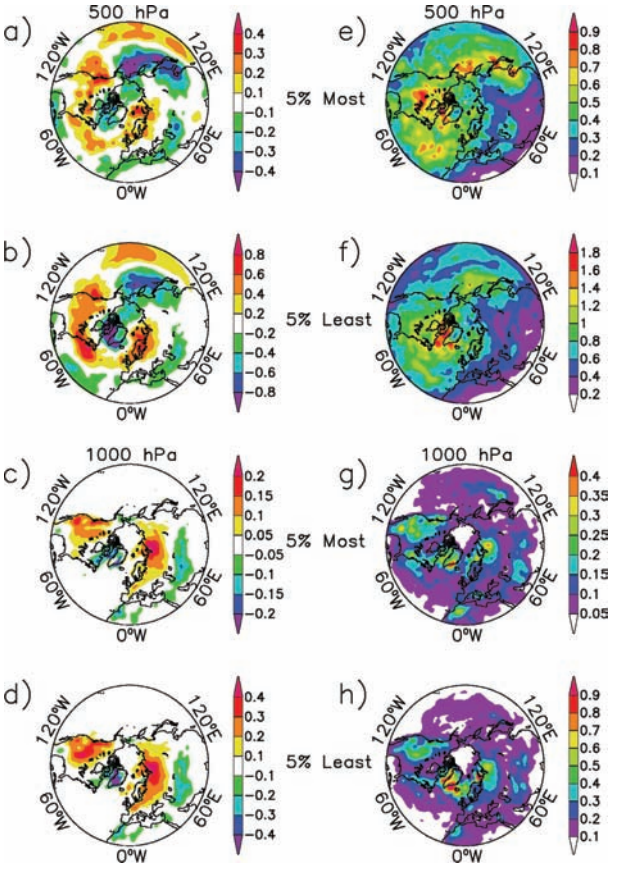

Fig. 6. Averaged (a)–(d) and rms (e)–(h) forcing sensitivity patterns (FSP) for the 5% most—(a), (c), (e) and (g)—and least—(b), (d), (f) and (h)—sensitive days. Shown are temperature tendency perturbations (K d^{-1}) in the mid-troposphere (model level 39)—(a), (b), (e) and (f)—and immediately above the ground surface (model level 60)—(c), (d), (g) and (h). The averaging employs the sensitivity indices as weights.

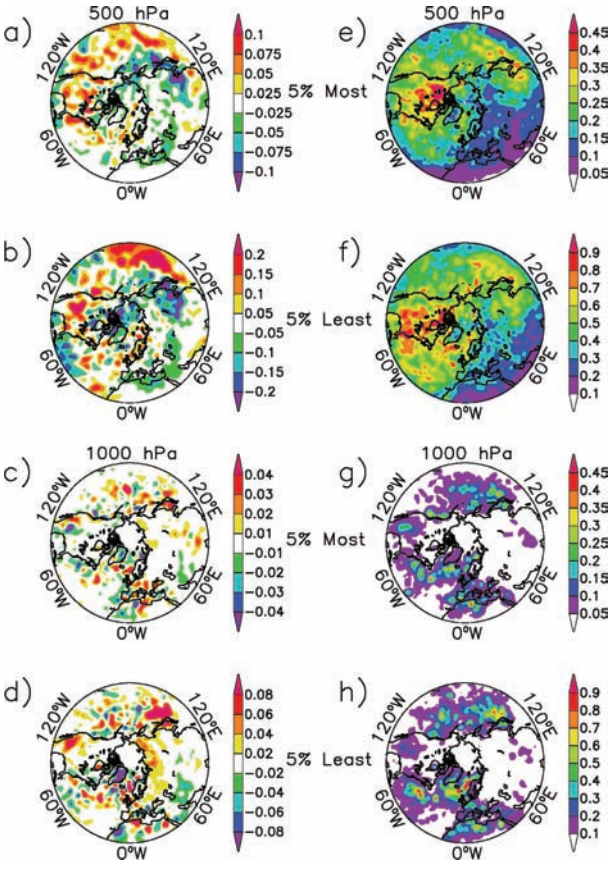

Fig. 7. Same as Fig. 6 but for initial sensitivity patterns (ISP) for temperature (K).

will gradually approach γ, for example if the optimization time equals one model time-step.

3.2. *Characteristics of the COWL sensitivity patterns*

Figures 6 and 7 respectively show statistics for FSP and ISP associated with the 5% most and 5% least sensitive cases. The mapped variables are the average and root mean square (rms) of temperature at model levels 39 (∼500 hPa) and 60 (lowest level above ground). The perturbation patterns are mainly located on the NH, and the larger values are located well inside the target area north of 30°N. Both for the forcing and the initial state perturbations the average is generally small compared to the rms, hence the variability is dominating over the averages and the rms nearly equals the standard deviation.

The average FSP resembles the COWL regime pattern shown in Fig. 2. The significance of this is further discussed in Section 5.1. It is also noted that the least sensitive cases both

have larger amplitudes and higher spatial correlation with the COWL regime pattern than the most sensitive cases. Higher initial and forcing amplitudes are imposed for low sensitivities in order to compensate for the slower growth. The higher spatial correlation possibly reflects a higher degree of predictability, as discussed in Section 5.2. The rms points to regions where the forcing perturbations are large and/or have high frequency of occurrence. Nevertheless, for a given atmospheric state other regions also have considerable perturbations but less consistently.

Figure 6 indicates that the FSPs are more uniform in the mid-troposphere than close to the surface. Near the surface some areas experience considerably higher rms-values than others, such that over the northern North-Atlantic and northern Eurasia. In the mid-troposphere the main contributions are from East Asia, the costal areas of The Pacific Ocean, north-eastern North-America, and The North-Atlantic Ocean. Even though rms-values for high CSI is higher over larger areas, the pattern of rms associated with high CSI resemble in many respects those associated with low. This might suggest that our sample of high CSI cases is not representative of the truly high sensitivity cases. However, the differences are important in that the atmosphere during high CSI is sensitive in more localized regions, in accordance with suggestions by Palmer (1999).

The ISPs have smaller spatial scales than the FSPs, and thus appear more chaotic. This agrees with the findings in Barkmeijer et al. (2003) and Iversen et al. (2003); while singular vectors develop upscale, forcing singular vectors have comparable spatial scales throughout the optimization time interval. In line with this, the resemblance of the average ISP with the COWL regime pattern is much weaker than for the average FSP. There is a significant amount of energy on the small scales. Iversen et al. (2006) showed that the detection of the high sensitivity cases depends on the horizontal resolution of the adjoint model, and that the ISP become even more small scale with increasing horizontal resolution, indicating a fundamental scale difference between the ISP and FSP. This could be expected since both patterns are constructed to yield a response pattern defined from monthly atmospheric anomalies, and given that the ISP is imposed only once in the beginning of the optimization time interval, while FSP is a continuous impact.

As for the FSP, the ISP perturbations are more wide-spread in the mid-atmosphere than close to the surface. Furthermore, the ISP perturbations have larger remote contributions than the FSP perturbations, and extend into the tropics. Large contributions are found close to the surface over oceans, but the Pacific and Atlantic Oceans are about equally important. There are only small perturbations over the continents except for Northern Africa and South-West Europe. Both FSP and ISP on the average are largest in the mid-troposphere, and decrease upwards and towards the surface (not shown). This is reflected in Figs. 6 and 7 where the peak values and the spatial extension are larger at 500 hPa than close to the surface.

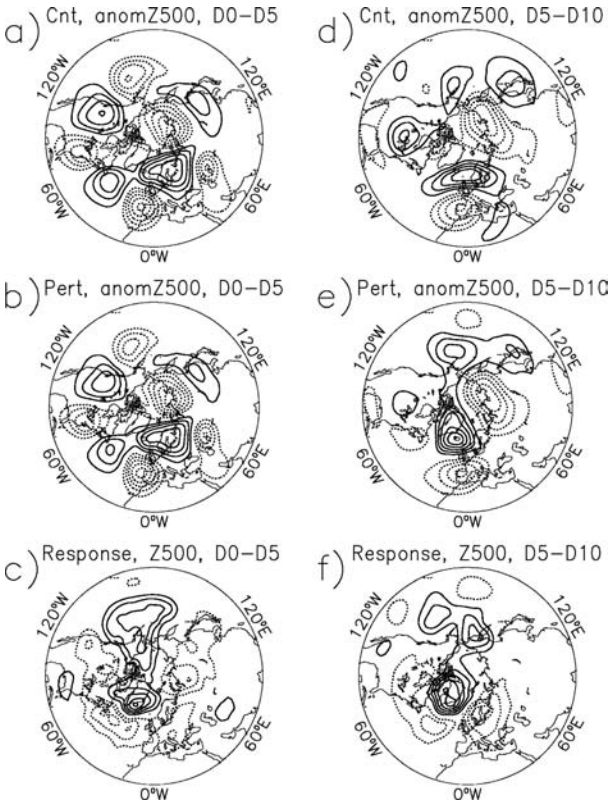

Fig. 8. Example of a single case where the non-linear model response to a 4-d FSP includes a pronounced shift of flow regime with respect to COWL. The model starts from 00 UTC 29 November 1963 with a COWL index of 2.59, and runs for the first 4 d with a forcing perturbation which is designed to decrease the projection on COWL, while the forcing is 0 thereafter up to day 10. Panels (a), (b) and (c) show 5-d averages of 500 hPa geopotential height anomalies over the first 5 d for the control run (every 50 m, COWL index 1.42), the perturbed run (every 50 m, COWL index 0.62), and for the difference (every 10 m). Panels (d), (e) and (f) show similar 5-d averages over the days 5–10 for the control run (every 50 m, COWL index −0.69), the perturbed run (every 50 m, COWL index −3.58), and for the difference (every 40 m).

4. Estimated atmospheric response

4.1. An example of forced COWL transition

Figure 8 shows results for one example starting from 12 UTC 29 November 1963. A clear change in the synoptic-scale circulation is seen in response to a FSP which is imposed over the first 4 d of a 10-d non-linear calculation with the ECMWF IFS. In order to focus on the time-scale for which the COWL regime pattern is not masked by daily variability, 5-d averages of the 500 hPa geopotential height anomalies relative to the ERA-40 climatology are shown in Fig. 8. Note that in this case the FSP for a negative COWL regime pattern is imposed; hence a response should show opposite sign than the pattern shown in Fig. 2a. The

southernmost latitude circle in Fig. 8 is 20°N. while in Fig. 2 it is 30°N.

The CI (in eq. 1) in the control run (top panels in Fig. 8) is 1.4 for the first 5-d average and −0.7 for the second 5-d average. Hence, there are already signs of an unforced change in the COWL regime in the control integration. In the perturbed run where the FSP is imposed over first 4 d, there is little change in the first 5-d average (CI = 0.6) but a considerable response for the second (CI = −3.6) even though the forcing is no longer imposed. Even the full anomaly in Fig. 8e) bear clear signatures of the pattern in Fig. 2a) with opposite sign. The response pattern, that is, the difference in anomalies between the perturbed and the control integration, shown in the lower panel is seen to correlate negatively with the pattern in Fig. 2a in the first 5-d period, but this is particularly more evident in the second (Fig. 8f). This behaviour indicates that the FSP occasionally can be regarded as a trigger of a regime change since sustained forcing is not required. However, the efficiency of FSP as a trigger is expected to vary from one case the other.

4.2. *Four-day response pattern*

Figure 9 shows the non-linear response in 500 hPa geopotential height at day 4 averaged over all 836 cases. The averaged non-linearly evolved perturbations at day 4 are very similar to the COWL regime pattern (Fig. 2a). The averaged spectral and vertical total dry energy profiles of the evolved perturbations (not shown) are also similar to the respective COWL profiles, and the response to the FSP shows the overall closest agreement. With a pattern scaling factor of $A = 10$ (see Section 2.4), the given side conditions in the iteration procedure cause the total energy norm of the average non-linear response pattern to be typically a factor 2–3 larger than the norm of γ_{COWL}. A suitable reduction of the amplitude of FSP or ISP will produce the correct norm.

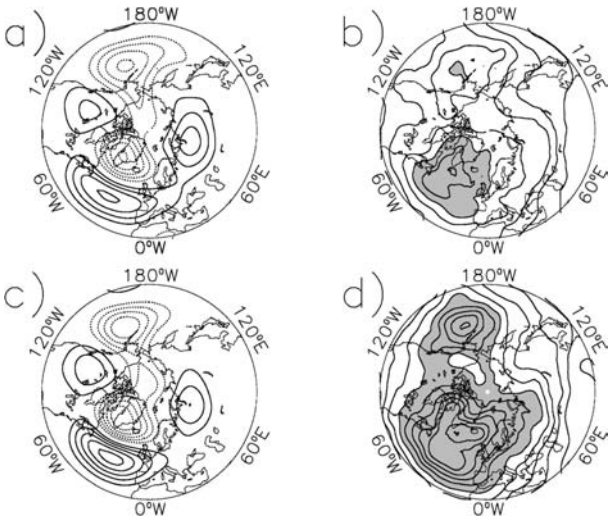

Fig. 9. Non-linearly evolved forcing, (a) and (b), and initial state, (c) and (d), perturbations at the end of the 4-d optimization time interval. The figure shows the average (a) and c) and standard deviation (b) and d) of the 500 hPa geopotential height (m) for all 836 individual cases from 22 extended winter seasons. For the averages the contours are drawn every 15 m and dashed curves represents negative values. For the standard deviation the contours are drawn every 4 m and the grey shading starts at 24 m.

The standard deviation map in Fig. 9 reflects a substantial variability in the 4-d response pattern. This variability is considerably larger and geographically more widespread for the evolved ISP (Fig. 9d) than for the evolved FSP (Fig. 9b), and it is particularly pronounced for the Pacific and Atlantic storm tracks. The standard deviation includes contributions both from fluctuations in the spatial patterns and in the amplitudes. A pure pattern resemblance can be estimated by the spatial correlations between the 836 cases and the original COWL pattern. The average correlation coefficient is 0.82 (0.75) for the non-linear response of the estimated optimal forcing (initial state) perturbations. Hence, about 67% (56%) of the spatial variance can be recognized by its resemblance with the COWL regime pattern, which supports the validity of the applied method.

4.3. *Four-day COWL index response*

The COWL regime index, CI, defined in eq. (1), measures the resemblance between a given atmospheric state and the pattern of the COWL regime. Simple flow indices are convenient because the values of a single scalar indicate the occurrence and approximate behaviour of a three-dimensional flow regime. The atmospheric response in the occurrence of the COWL regime at optimization time T (=4 d) to an imposed forcing for individual cases, is thus measured by the simple quantity $\Delta\,\mathrm{CI} = \mathrm{CI}\,(\mathbf{x}_T) - \mathrm{CI}\,(\mathbf{x}_T^c) = \mathrm{CI}\,(\mathbf{x}_T - \mathbf{x}_T^c)$, where $\mathbf{x}_T^c$ $(\mathbf{x}_T)$ is the control (perturbed) atmospheric development.

In its strictest definition, we define a COWL transition as a change in the sign of CI. Such transitions occur in 13 (7) of the 42 most (least) sensitive cases (see Table 1), and for a majority of these the CI changes from negative to positive. If we include transitions where CI changes sign at least twice during

Table 1. The number of COWL transitions between day 0 and day 4 in the 5% (42) high and low sensitivity composites. Results for both the basic state and perturbed trajectories are given. A COWL transition is defined as a change in the sign of the COWL index CI defined by eq. (1).

	Forcing sensitivity		Initial state sensitivity	
CSI-level	Basic state	Perturbed state	Basic state	Perturbed state
Highest 5%	12	17	13	18
Lowest 5%	7	11	7	10

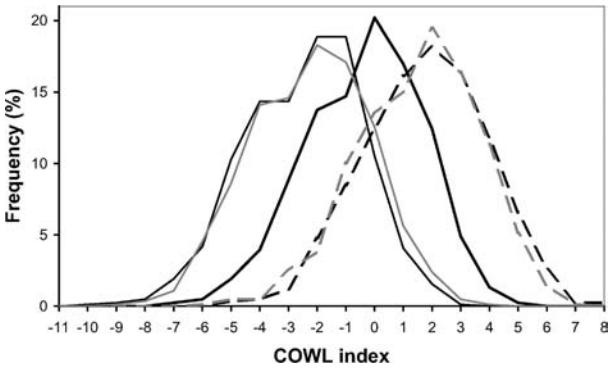

Fig. 10. Frequency distribution (%) of the COWL index for the unperturbed atmospheric states (thick black in the middle) and for non-linearly evolved states after optimally perturbing the model tendencies (forcing, thin black) or the initial states (grey). Results after subtracting perturbations are thin continuous curves to the left, and after adding perturbations are dashed curves to the right.

the 4 d optimization period, the number of high (low) sensitivity transitions increases by 5 (0). After adding optimal perturbations to the most sensitive cases, Table 1 shows that the COWL transitions increase from 13 to 18. Contra-intuitively, we find similar results also for the 5% least sensitive cases. This is, however, influenced by the experimental design which compensates the low sensitivity by increasing the amplitudes of the perturbations. The number of cases which is identified by COWL transition is probably too few to be statistically significant. In the discussions in this paper, we therefore include all changes in CI in positive or negative direction.

Figure 10 shows the frequency of occurrence of CI-values at optimization time (day 4) for the 836 atmospheric states employed in this study. In addition to showing the distribution of CI for the control calculations, two sets of frequency distributions for non-linearly evolved perturbed states are shown, one after adding optimal perturbations (dashed), and one after subtracting optimal perturbations (thin continuous). The frequency distribution for the control calculations indicates that a negative CI is climatologically about equally as likely as a positive CI. The distribution of the CI after perturbing with FSP (or ISP) have similar shapes but are significantly shifted along the axis for the CI in agreement with the sign of the added perturbations. This further supports the validity of the applied method for optimal perturbations.

4.4. *Response studies for high sensitivity cases*

Atmospheric states which are sensitive to small perturbations do not necessarily develop subsequent flow regime transitions. To trigger a COWL pattern response, an actual imposed forcing needs to project onto the FSP during the time slots when the CSI is large. In the following we discuss the properties of the FSP for the 10 cases with highest CSI. These cases are listed in Table 2. Seven of these are also among the 10 cases with the highest CSI for ISP, and the remaining 3 are among the 3% most sensitive. (The FSPs presented in Fig. 13 are discussed in Section 5.)

Table 2. The 10 most sensitive cases and their sensitivity indices scaled by their respective overall averages. The cases are ranked according to their sensitivity, and the dates are day N in the time interval [N, N + 4 d].

Forcing sensitivity		Initial state sensitivity	
Date	Sensitivity index	Date	Sensitivity index
Jan. 26 1989	2.1	Jan. 26 1989	2.6
Mar. 14 1980	1.7	Jan. 9 1980	2.2
Nov. 22 1970	1.6	Mar. 14 1980	2.1
Apr. 6 1971	1.5	Nov. 25 1977	2.0
Nov. 15 1997	1.5	Apr. 6 1971	1.9
Nov. 25 1977	1.5	Nov. 15 1997	1.8
Nov. 27 1989	1.5	Apr. 16 1990	1.8
Feb. 24 1993	1.5	Mar. 1 1993	1.8
Mar. 1 1993	1.5	Jan. 21 1992	1.8
Jan. 9 1980	1.5	Nov. 28 1964	1.7

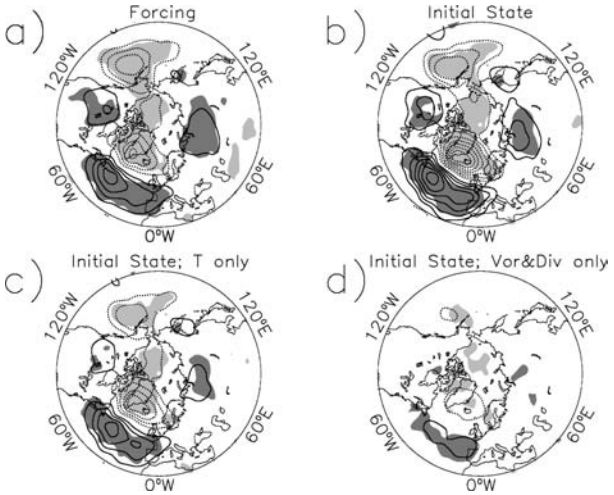

Fig. 11. Various D + 4 non-linearly evolved forcing and initial state perturbations, for the geopotential height anomalies at 500 hPa averaged over the 10 most sensitive cases (cf. Table 2). The equidistance is 15 m, negative values are dashed, and significant values at the 5% level are shaded. (a) Evolved FSP; (b) evolved ISP; (c) evolved ISP when only initial temperatures are perturbed; (d) evolved ISP when only initial vorticity and divergence are perturbed.

The average of the non-linear response over these cases is shown in Fig. 11a) for FSP and (b) for ISP, including estimates of 5% significance levels (two-sided *t*-test). The average response pattern clearly resembles that of the COWL regime in both cases. The amplitude is slightly smaller than the composite for all cases in Fig. 2. The main reason for this is that the iteration procedure

to evaluate the FSP compensates the quick growth of amplitudes when CSI is large, and that synoptic features occurring at the actual dates mask the monthly-scale COWL regime pattern more efficiently for statistics over 10 d than for the entire sample. However, the fractional amount of kinetic energy in the response anomaly pattern is ca. 75%, in good agreement with that of COWL regime pattern itself.

The relative importance of perturbing the atmospheric wind fields (i.e. vorticity and divergence) compared to the temperature fields in the ISP is shown for the 10 cases in Figs. 11c and d). The experiments are conducted by retaining only one of the two sets of variables in the ISP when calculating the non-linear response. The figures show that temperature perturbations alone are able to trigger a response pattern similar to the COWL regime. Both the spectral and vertical evolved total and kinetic energy profiles are identical to those obtained for the total ISP (not shown), even though only on the average 54% of the total energy in the response pattern is retained. In contrast, the experiment for which only the wind fields are perturbed yield a much weaker response, and the average evolved total energy is only about 19% of that obtained when using the total ISP. However, the kinetic energy constitutes about only 25% of the total energy for the complete ISP, hence the temperature and wind field perturbations are about equally efficient in initiating perturbation growth. The response pattern bears clear signatures of COWL, however, and the shapes of the vertical and spectral energy profiles are similar to that of the total optimal perturbations (not shown).

The simple energy budget above shows that the individual response patterns obtained for momentum and temperature initial perturbations separately, can not be added to yield the total simultaneous response. Hence, a significant portion of the non-linear response to the complete ISP perturbation stems from constructive interactions between the temperature and the wind fields during evolution of the ISP. Separate tests confirm that the response is more pronounced by including vorticity and divergence in the initial state perturbations rather than by increasing the magnitude of the temperature perturbation in the experiment without wind perturbations. Similar interferences were discussed for geostrophic and ageostrophic structures of singular vector evolution by Errico (2000).

For FSP perturbations the response to the temperature tendencies alone accounts for nearly 80% of the total energy obtained in the response to the complete FSP. Also in this case, the response patterns clearly resemble those of the response to the complete FSP (not shown). (Similar experiment for perturbing only vorticity and divergence tendencies in the FSP is inconclusive due to large truncation errors in vorticity and divergence in the file storage of FSP.)

4.5. Climatic response

We have seen that the estimated FSPs (and the ISPs) are able to efficiently influence the atmospheric development in the direction of a COWL regime pattern over 4 d. To what extent such forcing patterns have any climate significance is a more profound question. A given external forcing on the atmosphere may intermittently project efficiently and with the same sign onto FSP during occasions with high sensitivity. The occurrence of the COWL regime will thus change for a limited period after each occasion, such as shown for the single case in Fig. 8. It is only if a forcing projects onto the FSP with a preferred sign over extended periods that a systematic climate response should be expected.

In this section we perform some experiments to investigate if sustained changes in COWL regime occurrence can be obtained. The experiments are along the lines presented in Jung and Barkmeijer (2006) and Greatbatch and Jung (2007). The reason for studying the COWL regime in the first place is its potential role in the global climate change in recent decades (Corti et al., 1999). The possible anthropogenic forcing producing such a response is mainly a temperature tendency associated with radiation. We therefore, use the mean temperature component of the FSP in this experiment (see Fig. 6).

A 17-member ensemble of winter calculations is calculated. Each of the 17 calculations is 5 months long and starts from ERA-40 re-analysis data (operational ECMWF after 2002) on 1 November for the period 1990–2006. Observed SSTs were used as lower boundary conditions. Three sets of ensembles are made. A control ensemble is obtained by running the currently operational ECMWF IFS (cycle 32r2) with resolution T63L60, while a pair of additional ensembles is produced by respectively adding and subtracting the temperature part of the FSP averaged over the 42 cases with the 5% highest forcing sensitivity (CSI). Result statistics are made for the 17 four-month periods December through March, discarding the first months of each season as spin-up.

The resulting climate response is shown in Fig. 12. The ensemble averaged fields show significant anomalies in agreement with most features of the COWL regime pattern (Fig. 2). The resemblance is clearly smaller than the average over that obtained immediately after imposing momentary FSP for every individual cases (Figs. 9 and 11), including a slight eastward (downstream) shift for the positive FSP perturbation. The pattern in Fig. 9 should be regarded as being close to the maximum attainable resemblance with the COWL regime pattern. As discussed in Section 4.4, the pure temperature perturbation is slightly suboptimal for each individual case. Imposing the forcing averaged over 42 cases is probably also suboptimal, as further discussed in Section 5.1. Furthermore, in a climate response setting, the 4-d optimization time probably underestimates remote forcing contributions. Finally, the data used to define the COWL regime pattern is not taken from the model used for calculating the climate response, and the model's COWL regime may differ from the pattern we have defined. Overall, however, the climate response pattern in Fig. 12 confirms the usefulness of the applied method.

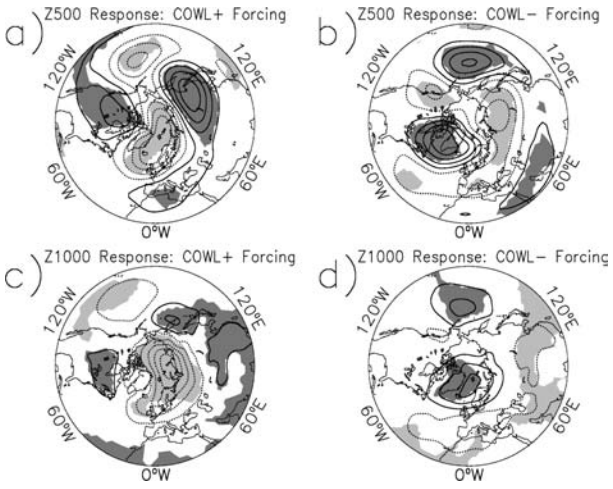

Fig. 12. Average climate response over 17 winter seasons (December–March) in geopotential height of 500 hPa (a and b) and 1000 hPa (c and d) to a constant temperature forcing achieved by averaging the temperature component of FSP over the 5% most sensitive cases (see Fig. 6). In (a) and (c) the response is to a FSP for positive COWL index (CI), while in (b) and (d) the response is to a FSP for negative CI. Changes relative to the unforced control integration are shown with 20 m equidistance. Negative contour lines are dashed. Hatched areas signify changes that are significant on the 5% level.

4.6. The assumption of tangent linearity

The procedure of calculating FSP and ISP is linear. Since the atmospheric flows are governed by non-linear laws, the applicability of the method requires that the atmosphere behaves quasi-linearly over the optimization interval. Most of the results shown in the previous sections show that the calculated non-linear response over 4–10 d to ISP or FSP resembles the COWL regime pattern for a large sample of cases. This is actually the main purpose of the method, and the assumption of tangent-linearity is not a serious issue, even though non-linear extensions of the method (Oortwijn and Barkmeijer, 1995) may be even more optimal. However, this result will depend on the assumed amplitude of the perturbations and indirectly on the length of the optimization interval. Non-linearity can thus be shown to be important if the amplitudes are inflated by a pattern scaling factor $A = 40$ (Iversen et al., 2006).

If the full non-linear model behaves quasi-linearly, two perturbations of opposite sign should also yield almost identical non-linearly evolved patterns of opposite sign. By definition, high sensitive cases yield perturbations with large growth rates. Amongst the calculated perturbations, these have therefore the highest risk of being influenced non-linearly if the optimal patterns are given the same amplitude. We have thus studied the validity of the assumed tangent-linear evolution of the optimal sensitivity patterns for the 100 cases having the highest CSI. The results show that the non-linearly evolved perturbations with $A = 10$ depend negligibly on the sign of the perturbations (not shown). Since the assumption of quasi-linearity thus is fulfilled, the deviations of $\boldsymbol{x}_\mathrm{T} - \boldsymbol{x}_\mathrm{T}^\mathrm{c}$ from $\boldsymbol{\gamma}$ are not attributable to significant non-linear effects.

5. Palmer's non-linear dynamical perspective

We have already mentioned several elements of the non-linear dynamical perspective by Palmer (1993, 1999). In particular, it is important to confirm the two basic aspects of the non-linearity. The first is that the growth-rate of small perturbations varies with the actual atmospheric state, and the second is that linearization of non-linear advection terms causes non-normality. Non-normality implies that even a quasi-linear response pattern to an imposed perturbation differs considerably from the pattern of the perturbation (Palmer, 1999; Farrell and Ioannou, 1996a, b). The first aspect is well documented by Figs. 3, 6 and 7 (see also Fig. 13), showing that the CSI, the FSP and the ISP are all flow-dependent. The second aspects is recognized by comparing for example, Fig. 11a) with the corresponding 10-d FSP in Fig. 13. Both basic aspects are further discussed in Section 5.1.

We address two more components of the non-linear dynamical perspective in addition to the two basic aspects. The first is that the impact of a small imposed forcing is felt primarily when predictability is low. The second is that the influence of the small imposed forcing is felt strongest in localized regions which do not coincide with the regions of atmospheric response. A consequence of this is that atmospheric states during high sensitivity (CSI large) should differ considerably from states during low sensitivity, since sensitivity should be lower for states belonging to a flow regime dominating the response.

Another two components of the non-linear perspective are not fully addressed in this study. These are (a) that the climate response to a small imposed forcing is primarily manifested in terms of changes in the frequency of occurrence of flow regimes, and (b) that the geographical structure of the flow regimes is relatively unaffected by the small imposed forcing. Here (a) can be associated with non-normality and is relevant for the discussion in Section 5.1 below, where it is shown that the degree to which the response pattern over 4 d shows a signature of the COWL regime is highly dependent on the optimal 'forcing of the day'. The latter bears itself little resemblance with the 4-d response pattern. Even though this result is in favour of (a) above, both (a) and (b) should be further investigated by defining flow regime patterns from the model's own data, and the optimization time T should be varied.

5.1. Evidence for flow dependence and non-normality

The FSP for each of the 10 cases with highest CSI, are shown for the 500 hPa spatial pattern for temperature in Fig. 13, and for the spectral energy profiles at 50, 500 and 900 hPa in Fig. 14. The FSP averaged over the 10 most sensitive cases as well as over all 836 cases are also presented One notable feature

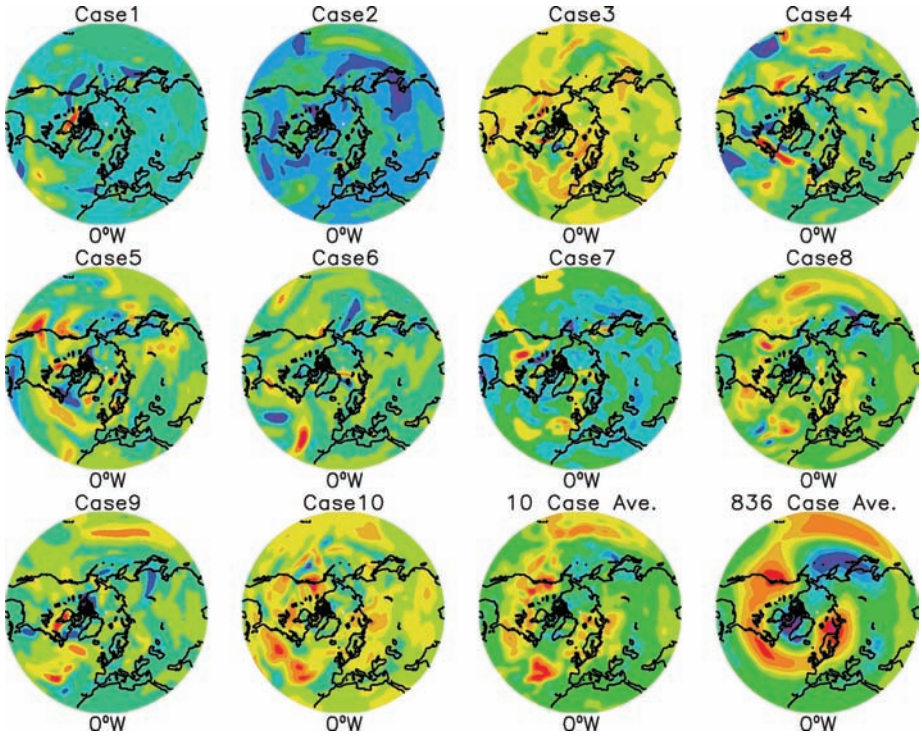

Fig. 13. The optimal temperature forcing perturbations for the 10 most sensitive cases at model level 39 (about 500 hPa). The average non-linear response corresponding to these forcing perturbations are shown in Fig. 11a. Also shown is the average over the 10 cases and over all 836 cases employed in this study (bottom right-hand side). The two averages have the same scaling (positive values are yellow to red and negative are green to blue), whereas the individual perturbations have arbitrary scaling. The vertically and horizontally integrated potential energy tendencies of the 10 most sensitive cases are in units μJs^{-2}: 0.066, 0.18, 0.73, 0.18, 0.25, 0.23, 0.61, 1.7, 0.31 and 1.1. The value for the 10-d average is 0.13 and for the 836-d average it is 0.37. Over 1 d, 1 μJs^{-2} equals about 7.5 kJ of energy.

is that the FSP are highly geographically localized, but the peak values differ both in magnitude, horizontal scale and location between the cases. Figure 14 shows that the energy is distributed over a wide range of horizontal scales but the wave number of the most energetic scales differ between the cases. In the stratosphere (50 hPa) the energy is mainly found on the largest scales with less case-to-case variability than in the troposphere. Spatial correlation between the individual cases confirms this, which is consistent with results in Jung and Barkmeijer (2006). We also find that the average FSP for COWL at 50 hPa resembles the NAO sensitivity pattern identified in Jung and Barkmeijer (2006).

The average over 836 cases is smooth and resembles the COWL pattern with a slight upstream displacement westwards. Non-normality should imply that finite-time optimal perturbations bear little resemblance with the atmospheric response. A sensitivity pattern vector decomposed onto strongly non-orthogonal normal modes for the tangent-linear model will rotate in the phase space, that is, change spatial pattern, over the optimization time due to different growth rates for the normal modes (Farrell and Ioannou, 1996a, b), and by construction end up with a maximum possible projection onto the COWL regime pattern. As a consequence of the averaging, the average FSP should produce a response with considerably weaker projections onto the COWL-pattern than the FSP for the individual cases.

In order to confirm the consequence of non-normality, we have perturbed each of the 10 most sensitive cases with the same average forcing perturbation. Both the mean taken over of all 836 cases and the mean over the 10 most sensitive cases are used. As seen in Figs. 15a and c, the evolved perturbations have considerably less in common with the COWL regime than those evolved from the case-specific FSP perturbations. Even though we recognize the COWL regime pattern in the response, the averaged FSPs are clearly far less optimal for response over 4 d than the momentary FSPs. For the 10 individual cases forced with the case-specific FSP (Fig. 11a), the spatial correlation between the COWL regime pattern and the response patterns (Fig. 11a) is typically around 0.7.

The very small amplitude of the response to the average FSPs can not be explained by the magnitude of these FSPs. Their amplitudes are in both cases comparable to those of the individual patterns (cf. Fig. 13). The growth of the perturbation norm is therefore considerably smaller than for the individual cases, indicating that the optimal forcing perturbations are strongly flow-dependent. Even taking the average over the 10 most sensitive cases and use this composite perturbation for the same 10 cases,

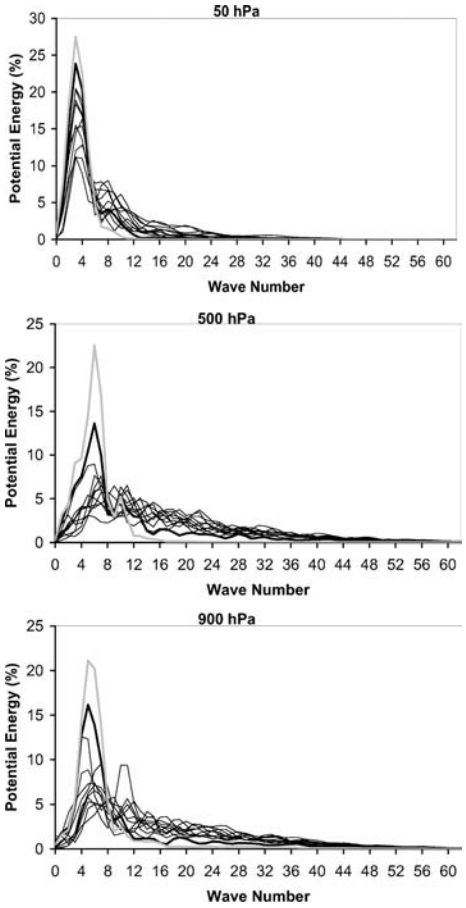

Fig. 14. Spectral distribution of potential energy for the 10 most sensitive forcing perturbations (thin black lines) for three model levels; Top: about 50 hPa; middle: about 500 hPa; and bottom: about 900 hPa. The spectra of the average sensitivity pattern are plotted as a thick black line and the average taken over all 836 optimal forcing perturbations are presented in grey. The profiles are given as percentages of the respective horizontally integrated potential energy.

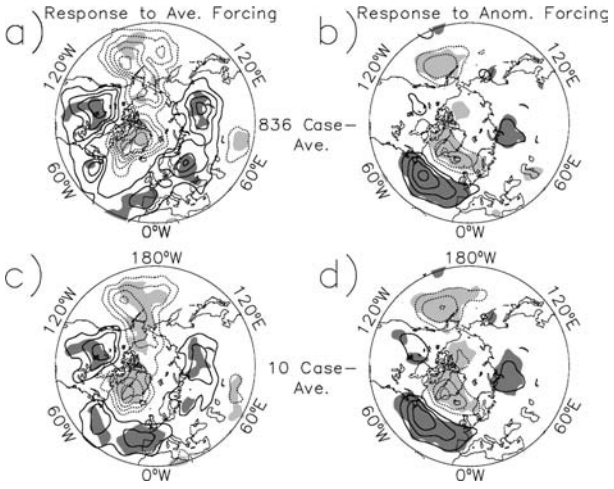

Fig. 15. Non-linearly evolved perturbations at D + 4 shown as geopotential height at 500 hPa for the days with the 10 highest CSI. The average responses over the 10 cases are shown. In (a) and (c) each of the 10 cases are perturbed with the FSP for COWL averaged over the entire set of 836 cases (a), and over the 10 most sensitive cases only (c). In (b) and (d) the response is calculates when daily anomalies in the FSP are used as forcing. The contours are drawn every 3 m in (a) and (c), and every 15 m in (b) and (d). Grey shadings show 5% significant signals.

destroys most of the optimal properties which are responsible for perturbation growth. This is further emphasized in experiments which use the deviations in FSP from the two alternative averages as forcing perturbation in each case (Figs. 15b and d). In this case, the averaged responses have ca. five times larger amplitude and correlate well with the COWL pattern. The response is close to that of the total optimal perturbations (cf. Fig. 11a), with spatial correlation of about 0.96. The spatial correlation of the FSP with the COWL regime pattern is typically about 0.3. This correlation is obviously smaller (larger) for the anomaly (average) FSPs. Hence the FSP perturbations which most efficiently change the atmospheric states towards the COWL regime pattern, has little spatial correlation with the COWL pattern itself, in accordance with the non-normality of the tangent-linear model.

The results in this section may appear to be in contradiction to the results in Section 4.5, where climate responses to average FSPs were discussed. The reason why the climate response show better pattern resemblance and response amplitude than for 4-d response calculations is not investigated in depth in this paper. Probably the much longer time for perturbation growth is an important factor. Another factor could be that over very many cases (17 seasons) it is also possible that the average FSP perturbation occasionally projects with significant components onto case-specific FSPs. Further investigation is needed in this area.

5.2. *High sensitivity – low predictability*

The next signature of the non-linear dynamical perspective we will investigate is the postulated relation between the system's sensitivity to external forcing and predictability of the atmospheric flows. Here we discuss sensitivity for forcing perturbations with respect to state transition to or from the COWL regime pattern. It is therefore the predictability of changes relative to the COWL pattern which is relevant for the discussion. Predictable transitions in the CI should be associated with low values of the CSI, and vice versa.

We have calculated predicted changes in CI over 4 d by the ECMWF IFS for control runs, that is, without any perturbation of the initial state or the model tendencies. These forecasts have been made for the 42 cases with highest CSI and the 42 cases with lowest CSI, where the CSI-values are with respect to forcing.

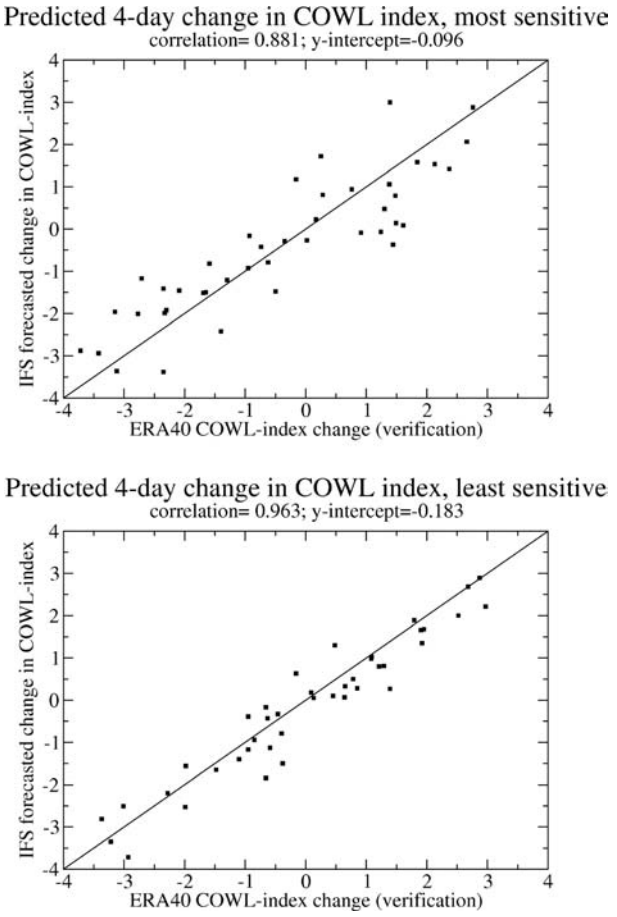

Fig. 16. Changes in COWL index (CI) is more predictable when sensitivity (CSI) is low than when it is high. Top panel shows a scatter-plot for predicted change in CI versus the ERA-40 analysed change in CI during the days with 5% highest CSI (correlation 0.881), while the bottom panel shows the same during the 5% least sensitive days (correlation 0.963).

The forecasts are verified against values of CI calculated from the ERA-40 data, by comparing 4-d forecasted changes in CI with analysed 4-d changes. Results are presented in the scatter plots in Fig. 16. The relation between sensitivity and reduced predictability is confirmed both visually and more quantitatively by the correlation coefficient between forecasted and observed CI change.

5.3. Basic state development and sensitivity

The final signature of the non-linear dynamical perspective investigated in this study concerns the atmospheric states during high sensitivity (CSI) as opposed to low sensitivity. The two sets of states classified according to high or low CSI, should show different flow characteristics. In other words, they should occupy different sections of the attractor for atmospheric flows.

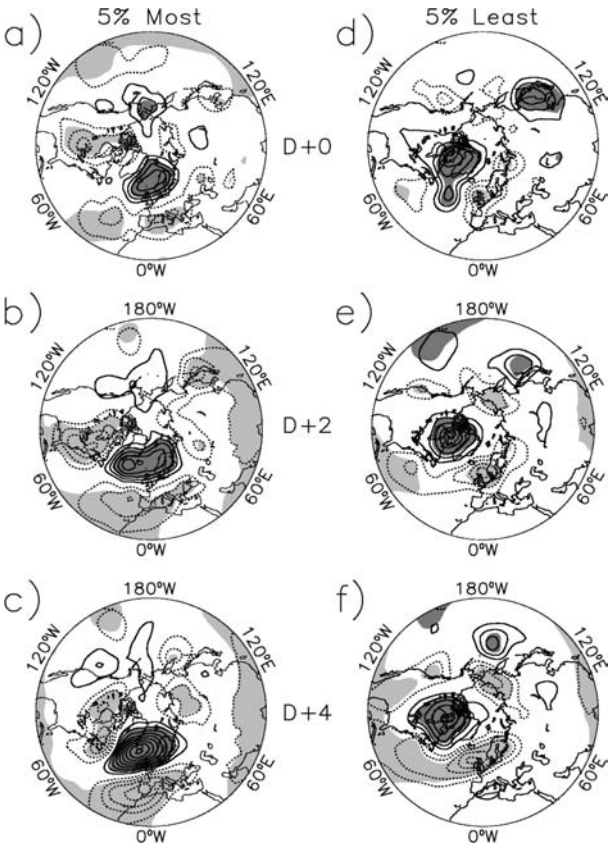

Fig. 17. Time evolution of the composite of basic states (control) which are the 5% most sensitive (a–c) and the 5% least sensitive (d–f) with respect to the FSP for COWL. Contour lines are anomalies in 500 hPa geopotential heights anomalies at day 0 (top row), day 2 (middle) and day 4 (bottom) in the optimization interval. The contour interval is 20 m and negative values are dashed. Shaded areas are significant anomalies at the 5% level.

Composites of basic state developments, that is, the control, have been made of those unperturbed atmospheric states in the sample which respectively have the 5% highest CSI and the 5% lowest CSI. There are 42 cases contributing to each composite. The anomaly patterns relative to climatology for these composites shown in Fig. 17 are thus either very sensitive (left-hand panels), or not so sensitive (right-hand panels), with respect to producing changes in the CI. The composite for the least sensitive cases shows signatures of a NAM, or AO, in its negative phase, thus resembling the Cluster D of Corti et al. (1999). The composite for the most sensitive cases shows signatures of an Atlantic-European dipole reminiscent of a negative-phase NAO. This is the opposite of the NAO-pattern associated with cluster A in Corti et al. (1999). Furthermore, there are signatures of a positive-phase Pacific North-American pattern (PNA). Both these features are characteristic for cluster B in Corti et al. (1999) with a negative sign.

Since the most sensitive cases are dominated by a development with a large negative NAO index and that our COWL regime

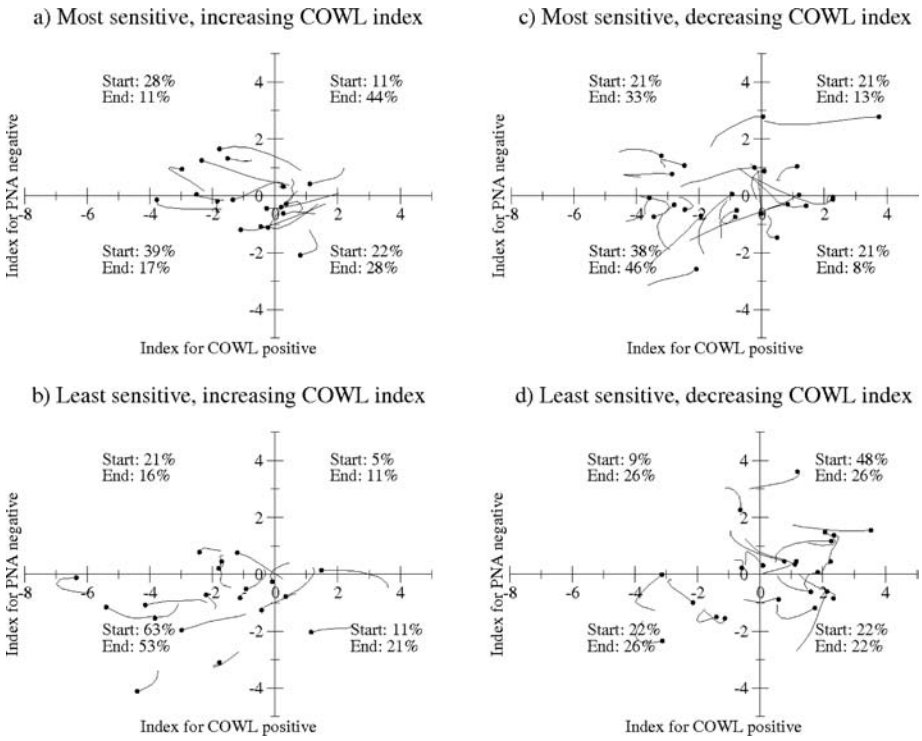

Fig. 18. 10-d trajectories for basic atmospheric states presented in a two-dimensional phase space of flow regime indices for the Corti et al. (1999) clusters A (COWL+) along the *x*-axis and B (PNA–) along the *y*-axis. The trajectory positions are smoothed by applying a 5-d moving average. Trajectories with increasing COWL index are shown in (a) and (b); while those with decreasing COWL index are shown in (c) and (d). The trajectories in panels (a) and (c) to the left-hand side belong to the 5% most sensitive cases; the trajectories on the panels (b) and (d) to the right-hand side belong to the 5% least sensitive cases. Statistics for start- and end-points of the trajectories are given in each quadrant.

pattern has a strong positive NAO index, the calculated FSP tend to hamper transitions away from the COWL regime. This is consistent with the results of Iversen et al. (2003) using the three-level T21 QG model, and similar results were also found for the most sensitive atmospheric states for the PNA identified by Corti and Palmer (1997) with the same model. Based on this, it appears that the atmospheric flows can be classified in different modes of variability during high and low sensitivity with respect to the COWL regime. This is confirmed to a large extent in Fig. 18, which shows a representation of the atmospheric flow developments as trajectories in a 'phase space' defined by the COWL and the PNA patterns. The values on the two axes are the projections onto cluster A (the CI: index for positive COWL and NAO) and cluster B (index for negative PNA and negative NAO). These were shown to be quasi-orthogonal in Corti et al. (1999). Each case is represented with a trajectory for the 10-d control integration after applying a 5-d moving average operator which filters progressive synoptic features in order to emphasize flow regimes (cf. Fig. 8).

From Fig. 18 one see that the most sensitive developments lie predominantly in other regions of the 'phase space' than the least sensitive. For increasing CI (Fig. 18), the most sensitive cases generally have smaller projections onto the two clusters than the least sensitive, which more often have a negative CI and a positive index for PNA. For decreasing CI the picture is slightly more complicated. The most sensitive cases tend to have a negative CI and no particular index trend for PNA, while the least sensitive mainly have positive CI and a slightly negative index for PNA. Given the highly truncated representation of these results, we take these results as indicative of systematic differences in atmospheric flows between cases of high and low sensitivity.

6. Summary and conclusions

This paper presents and discusses optimal forcing perturbations, or FSP, which produce an atmospheric response over 4 d which resembles the northern hemispheric COWL regime pattern, as represented by cluster A of Corti et al. (1999). Related optimal initial state perturbations, or initial sensitivity patterns (ISP) are included for comparison. As opposed to the previous simpler model studies of, for example, Corti and Palmer (1997) and Iversen et al. (2003), this study uses the ECMWF IFS atmospheric global model with T63L60 resolution and full physics. A total of 836 cases during 22 winter seasons in the period 1957–2002 have been used for calculations of FSP and ISP perturbations. The method is generalized from Klinker et al. (1998) and Barkmeijer et al. (2003), and is also used in Jung and Barkmeijer (2006) and Greatbatch and Jung (2007).

The reason for choosing the COWL regime pattern is its potential relevance for climate change during the last —four to five decades, as shown by Corti et al. (1999). An optimal forcing for COWL may therefore be an ingredient in the explanation of observed climate change in terms of changed relative occurrence of flow regimes. Such interpretations should, however, be applied with caution. The FSP is purely atmospheric, and it does not separate interactions with other parts of the climate system (e.g. the oceans) from radiative interactions with the universe. Furthermore, because of the limited time range of 4 d, remote components (e.g. tropical) to the optimal forcing perturbations are not explicitly included.

The CSI, which measures how large a perturbation a unit length forcing produces over the optimization time of 4 d, varies considerably with the atmospheric state, and the variability is larger for initial perturbations than for forcing. The frequency distributions are skewed with elongated tails towards high values. The temporal correlation between forcing CSI and initial CSI is high (0.91). High sensitivities occur intermittently with short duration. The FSP has larger spatial scales than the ISP, and averaged over many cases the FSP resembles the COWL regime pattern. This is not the case for the ISP. Both the average ISP and its variability are geographically more widespread than the FSP. Hence, remote and small-scale influences appear to be more important for initial state perturbations than for forcing perturbations.

The method has proven efficient in providing flow-dependant perturbations in forcing and initial data which produce an atmospheric response which resembles the COWL regime pattern. This resemblance is established by subjective pattern recognition, by calculating projections with the total energy inner product (the CI), and by calculating spatial correlations. About 2/3 of the variance of the 4-d response to the FSP is recognized by its resemblance with the COWL regime pattern. The similar number for ISP is a little more than 1/2. The number of COWL regime transitions over 4 d is too small to be statistically significant, but the frequency distributions of CI show a significant response.

The efficiency in producing response in CI over 4 d is highly dependent on using the exact forcing valid for the actual dates. Averaging the FSP over only the 10 most sensitive cases (out of 836), reduces the efficiency considerably. Hence, the climate significance of a forcing which is relatively invariant can be important if it intermittently projects onto the FSP in a consistent manner. Alternatively, the response pattern may generally develop more slowly and only in relatively rare occasions be subject to abrupt changes. A preliminary test with a perpetual winter climate response, a forcing averaged over 5% most sensitive cases does produce a response which resembles the COWL regime pattern. Experiments beyond the scope of this paper will be needed to uncover the reason for this. Further experiments are also needed to confirm a constructive interference between temperature and wind-field perturbations seen for a small sample of 10 cases.

The paper discusses selected elements in the non-linear dynamical perspective of climate change proposed by Palmer (1993, 1999). Two basic aspects of non-linearity are confirmed by our calculations. The flow dependence of growth rates of small perturbations has been verified, as well as the non-normality of the tangent-linear model due to linearized advection. One consequence of non-normality is that the response pattern deviates considerably from the pattern of the imposed forcing (e.g. the FSP). Two more elements of the non-linear dynamical perspective have also been confirmed. First, we have documented that sensitive states have systematically smaller predictability than less sensitive states. Second, we have shown clear indications that the most sensitive states have different flow characteristics with respect to known flow regime patterns (PNA, NAO and COWL), than the least sensitive. Two final elements are not fully discussed in this paper. First, the climate response to a small imposed forcing is postulated to primarily manifest in terms of changes in the frequency of occurrence of flow regimes. Second, the geographical structure of the flow regimes is relatively unaffected by the small imposed forcing. Even though we have seen results in support of the first, these items need to be based on full climate impact experiments where flow regime patterns and their occurrence are estimated directly from the climate model's own output.

Our results may shed light onto the potential usefulness of regional climate models (RCMs) designed for downscaling global climate scenarios (e.g. Giorgi et al., 2001; see also Haugen and Iversen, 2008; Køltzow et al., 2008). Various external and internal forcing terms are calculated with more spatial detail in RCMs than in the driving GCMs. If the RCM domains include local areas with occasional high forcing sensitivity, improved geographical features in the RCMs will potentially improve the downscaled climate. Important optimal forcing features connected with high sensitivity have considerable amplitudes locally (as opposed to remotely). Hence, if the resolved scale forcing structures inside the RCM integration domain are improved, a well designed RCM should produce improved results.

The issue of boundary layer forcing perturbations relative to those in the free troposphere and above, has also been tentatively addressed in this study (not shown); preliminary results suggest that the boundary layer forcing over the North Atlantic Ocean may be important for the frequency of occurrence of the COWL regime. This will be further investigated. Furthermore, targeting of the forcing perturbations to other vertically or horizontally defined regions, or to selected model variables, will be pursued in future work.

7. Acknowledgement

This work is a part of the RegClim project, and later NorClim, financed by the Research Council of Norway under the NorKlima Programme. Computer resources to this project have been granted through the Special Project SPNOREGC at ECMWF.

We are grateful to Dr. T. N. Palmer who provided initial ideas and intellectual momentum to this work. Dr. S. Corti kindly provided the data for the 500 hPa flow regime patterns, and discussions with Dr. I.-L. Frogner are much appreciated. We also thank the two anonymous reviewers for exceptionally valuable suggestions.

References

Barkmeijer, J., Iversen, T. and Palmer, T. N. 2003. Forcing singular vectors and other sensitive model structures. *Quart. J. Roy. Meteor. Soc.* **129**, 2401–2423.

Blackmon, M. L. 1976. A climatological spectral study of the 500mb geopotential height of the Northern Hemisphere. *J. Atmos. Sci.* **33**, 1607–1623.

Boer, G. J. and Yu, B. 2003. Climate sensitivity and response. *Clim. Dyn.* **20**, 415–429, doi: 10.1007/s00382-002-0283-3.

Branstator, G. 1990. Low-frequency patterns induced by stationary waves. *J. Atmos. Sci.* **47**, 629–648.

Branstator, G. 2002. Circumglobal teleconnections, the jet stream waveguide, and the North Atlantic oscillation. *J. Climate* **15**, 1893–1910.

Broccoli, A. J., Lau, N.-C. and Nath, M. J. 1998. The cold ocean-warm land pattern: model simulation and relevance to climate change detection. *J. Climate* **11**, 2743–2763.

Buizza, R. 1993. Impact of a simple vertical diffusion scheme and of the optimization time interval on optimal unstable perturbations. ECMWF Research Department Technical Memorandum no. 192, ECMWF, Shinfield Park, Reading RG2 9AX, United Kingdom.

Buizza, R. 1994. Localization of optimal perturbations using a projection operator. *Quart. J. Roy. Meteor. Soc.* **120**, 1647–1682.

Buizza, R. and Palmer, T. N. 1995. The singular-vector structure of the atmospheric global circulation. *J. Atmos. Sci.* **52**, 1434–1456.

Cheng, X. and Wallace, J. M. 1993. Cluster analysis of the Northern Hemisphere wintertime 500-hPa height fireld: spatial patterns. *J. Atmos. Sci.* **50**, 2674–2696

Corti, S. and Palmer, T. N. 1997. Sensitivity analysis of atmospheric low-frequency variability. *Quart. J. Roy. Meteor. Soc.* **123**, 2425–2447.

Corti, S., Molteni, F. and Palmer, T. N. 1999. Signature of recent climate change in frequencies of natural atmospheric circulation regimes. *Nature* **398**, 799–802.

Ehrendorfer, M., Errico, R. and Gelaro, R. 1999. Singular-vector perturbation growth in a primitive equation model with moist physics. *J. Atmos. Sci.* **47**, 1627–1648.

Errico, R. M. 1997. What is an adjoint model? *Bull. Amer. Meteor. Soc.* **78**, 2577–2591.

Errico, R. M. 2000. The dynamical balance of singular vectors in a primitive equation model. *Quart. J. Roy. Meteor. Soc.* **126A**, 1601–1618.

Evans, K. J. and Black, R. X. 2003. Piecewise tendency diagnosis of weather regime transitions. *J. Atmos. Sci.* **60**, 1941–1959

Farrell, B. F. and Ioannou, P. J. 1996a. Generalized stability theory. Part I: autonomous operators. *J. Atmos. Sci.* **53**, 2025–2040.

Farrell, B. F. and Ioannou, P. J. 1996b. Generalized stability theory. Part II: nonautonomous systems. *J. Atmos. Sci.* **53**, 2042–2053.

Giorgi, F., Hewitson, B., Christensen, J., Hulme, M., von Storch, H., and co-authors. 2001. Regional climate information. evaluation and projections. In: *Climate Change 2001: The Scientific Basis. Contribution of Working Group I to the Third Assessment Report of the Intergovernmental Panel of Climate Change* (eds J. T. Houghton, D. J. Griggs, M. Noguer, P. J. van der Linden, X. Dai, K. Maskell and C. A. Johnson). Cambridge University Press, Cambridge, United Kingdom.

Greatbatch, R. J. and Jung, T. 2007. Local versus tropical diabatic heating and the winter North Atlantic Oscillation. *J. Climate* **20**, 2058–2075.

Haugen, J. E. and Iversen, T. 2008. Response in extremes of daily precipitation and wind from a downscaled multi-model ensemble of anthropogenic global climate change scenarios. *Tellus* **60A**, this issue.

Hasselmann, K. 1993. Optimal fingerprints for the detection of time-dependent climate change. *J. Climate* **6**, 1957–1969.

Hurrell, J. W. 1996. Influence of variations in extratropical wintertime teleconnections on Northern Hemisphere temperature. *Geophys. Res.Lett.* **23**, 665–668.

Iversen, T., Barkmeijer, J. and Palmer, T. N. 2003. Optimal forcing perturbations for the atmosphere. *RegClim Phase III-General Technical Report* **7**, 107–135.

Iversen, T., Kristiansen, J., Jung, T. and Barkmeijer, J. 2006. Optimal forcing sensitivity patterns for changes in northern hemispheric flows in the atmosphere. *RegClim Phase III-General Technical Report* **9**, 21–49.

Jung, T. 2005. Systematic errors of the atmospheric circulation in the ECMWF forecasting system. *Quart. J. Roy. Meteorol. Soc.* **131**, 1045–1073.

Jung, T. and Barkmeijer, J. 2006. Sensitivity of the tropospheric circulation to changes in the strength of the stratospheric polar vortex. *Mon. Wea. Rev.* **134**, doi:10.1175/MWR3178.1.

Jung, T., Barkmeijer, J., Coutinho, M. M. and Mazeran, C. 2003. Sensitivities and singular vectors with moist norms. *ECMWF Workshop on Humidity Analysis*, Shinfield Park, Reading RG2 9AX, UK, 177–189.

Jung, T., Palmer, T. N. and Shutts, G. J. 2005. Influence of a stochastic parameterization on the frequency of occurrence of North Pacific weather regimes in the ECMWF model. *Geophys. Res. Lett.* **32**, L23811, doi:10.1029/2005GL024248.

Kanestrøm, I., Pedersen, K. and Skåtun, H. 1985. Major stationary ridges and troughs at 500mb. *Geophysica Norvegica* **33**, 1–40.

Kimoto, M. and Ghil, M. 1993. Multiple flow regimes in the Northern Hemisphere winter. Part I: methodology and hemispheric regimes. *J. Atmos. Sci.* **50**, 2625–2643.

Klinker, E., Rabier, F. and Gelaro, F. 1998. Estimation of key analysis errors using the adjoint technique. *Quart. J. Roy. Meteor. Soc.* **124**, 1909–1933.

Kumar, A. and Hoerling, M. P. 1998. On the specification of regional SSTs in AGCM simulations. *J. Geophys. Res.* **103**, 8901–8907.

Køltzow, M., Iversen, T. and Haugen, J. E. 2008. On abilities and limitations of atmospheric dynamical downscaling of global climate scenarios. *Tellus* **60A**, this issue.

Lejenäs, H. and Økland, H. 1983. Characteristics of northern hemispheric blocking as determined from long time-series of observational data. *Tellus* **35A**, 350–362.

Lorenz, E. N. 1963. Deterministic nonperiodic flow. *J. Atmos. Sci.* **20**, 130–141.

Lu, J., Greatbatch, R. J. and Peterson, K. A. 2004. Trend in Northern Hemisphere winter atmospheric circulation during the last half of the twentieth century. *J. Climate* **17**, 3745–3760.

Mahfouf, J.-F. 1999. influence of physical processes on the tangent-linear approximation. *Tellus* **51A**, 147–166.

Mo, K. C. and Ghil, M. 1988. Cluster analysis of multiple planetary flow regimes. *J. Geophys. Res.* **93**, 10927–10952.

Molteni, F., Tibaldi, S. and Palmer, T. N. 1990. Regimes in the wintertime circulation over northern extratropics I: observational evidence. *Quart. J. Roy. Meteor. Soc.* **124**, 495–526.

Molteni, F., Ferranti, L., Palmer, T. N. and Viterbo, P. 1993. A dynamical interpretation of the global response to equatorial Pacific SST anomalies. *J. Climate* **6**, 777–795.

Molteni, F., Kucharski, F. and Corti, S. 2006. On the predictability of flow-regime properties on interannual to interdecadal timescales. In: *Predictability of Weather and Climate* (eds T. N. Palmer and R. Hagedorn). Cambridge University Press, Cambridge, UK, pp. 365–390.

Moore, A. M. and Kleeman, R. 1999. Stochastic forcing of ENSO by the intraseasonal oscillation. *J. Climate* **12**, 1199–1220.

Moore, A. M., Zavala-Garay, J., Tang, Y., Kleeman, R., Weaver, A. T., and co-authors. 2006. Optimal forcing patterns for coupled models of ENSO. *J. Climate* **19**, doi:10.1175/JCLI3870.1.

Nese, J. M. 1989. Quantifying local predictability in phase space. *Physica* **D35**, 237–250.

Oortwijn, J. and Barkmeijer, J. 1995. Perturbations that optimally trigger weather regimes. *J. Atmos. Sci.* **52**, 3932–3944.

Orrell, D. 2002. Role of the metric in forecast error growth: how chaotic is the weather? *Tellus* **54A**, 350–362. doi:10.1034/j.1600-0870.2002.01389.x.

Orrell, D., Smith, L., Barkmeijer, J. and Palmer, T. N. 2001. Model error in weather forecasting. *Nonl. Process. Geophys.* **8**, 357–371.

Palmer, T. N. 1993. A nonlinear dynamical perspective on climate change. *Weather* **48**, 313–326.

Palmer, T. N. 1996. Predictability of the atmosphere and oceans: from days to decades. In: *Decadal Climate Variability Dynamics and Predictability* Volume **44**. NATO ASI Series, Springer, Berlin, Heidelberg, pp. 83–155.

Palmer, T. N. 1999. A nonlinear dynamical perspective on climate prediction. *J. Climate* **12**, 575–591.

Quadrelli, R. and Wallace, J. M. 2004. A simplified linear framework for interpreting patterns of northern hemisphere wintertime climate variability. *J. Clim.* **17**, 3728–3744.

Randall, D. A., Wood, R. A., Bony, S., Colman, R., Fichefet, T., and co-authors. 2007. Cilmate models and their evaluation. In: *Climate Change 2007. The Physical Science Basis. Contribution of Working Group I to the Fourth Assessment Report of the Intergovernmental Panel on Climate Change* (eds S. Solomon, D. Qin, M. Manning, Z. Chen, M. Marquis, and co-editors.). Cambridge University Press, Cambridge, United Kingdom and New York, NY, USA.

Rex, D. F. 1950. Blocking action in the middle troposphere and its effects upon regional climate II. The climatology of blocking action. *Tellus* **2**, 275–301.

Simmons, A. and Hollingsworth, A. 2002. Some aspects of the improvement of the skill of numerical weather prediction. *Quart. J. Roy. Meteor. Soc.* **128**, 647–677.

Smyth, P., Ide, K. and Ghil, M. 1999. Multiple regimes in Northern Hemisphere height fields via mixture model clustering. *J. Atmos. Sci.* **56**, 3704–3723.

Stephenson, D. B., Hannachi, A. and O'Neill, A. 2004. On the existence of multiple climate regimes. *Quart. J. Roy. Meteor. Soc.* **130**, 583–605.

Thompson, D. W. J. and Wallace, J. M. 1998. The Artic Oscillation signature in the wintertime geopotential height and temperature fields. *Geophys. Res. Lett.* **25**, 1297–1300.

Thompson, D. W. J. and Wallace, J. M. 2000. Annular modes in the extratropical circulation. Part I: month-to-month variability. *J. Clim.* **13**, 1000–1016.

Uppala, S. M., Kållberg, P. W., Simmons, A. J., Andrae, U., da Costa Bechtold, and co-authors. 2005. The ERA-40 re-analysis. *Quart. J. Roy. Meteorol. Soc.* **131**, 2961–3012. doi:10.1256/qj.04.176.

Wallace, J. M. 2000. North Atlantic Oscillation/annular mode: two paradigms-one phenomenon. *Q. J. Roy. Meteo. Soc.* **126**, 791–805.

Wallace, J. M. and Gutzler, D. S. 1981. Teleconnections in the geopotential height field during the Northern Hemispheric winter. *Mon. Wea. Rev.* **109**, 784–812.

Wallace, J. M., Zhang, Y. and Bajuk, L. 1996. Interpretation of interdecadal trends in Northern Hemispheric surface air temperature. *J. Climate* **9**, 249–259.

Wu, Q. and Straus, D. M. 2004a. On the existence of hemisphere-wide climate variations. *J. Geophys. Res.* **109**, D06118, doi:10.1029/2003JD004230.

Wu, Q. and Straus, D. M. 2004b. AO, COWL, and observed climate trends. *J. Climate* **17**, 2139–2156.